Local Dzyaloshinskii-Moriya Interactions Driving Quasi-2D Magnetism in a Centrosymmetric Nanoskyrmion Material

S. H. Moody,[1,2,3,*] P. J. Bereciartua,[4] S. Francoual,[4] M. T. Littlehales,[2,5] M. N. Wilson,[2,6] M. Gomilšek,[2,7,8] M. T. Birch,[9] D. A. Mayoh,[10] G. Balakrishnan,[10] and P. D. Hatton[2]

[1]*Laboratory for Neutron Scattering and Imaging (LNS), PSI Center for Neutron and Muon Science, Paul Scherrer Institut (PSI), CH-5232 Villigen, Switzerland*

[2]*Department of Physics, Durham University, South Road, Durham DH1 3LE, United Kingdom*

[3]*Department for Hydrogen Technology, Institute for Energy Technology, Kjeller NO-2027, Norway*

[4]*Deutsches Elektronen-Synchrotron DESY, Hamburg 22607, Germany*

[5]*ISIS Neutron and Muon Source, Rutherford Appleton Laboratory, Didcot OX11 0QX, United Kingdom*

[6]*Department of Physics and Physical Oceanography, Memorial University of Newfoundland, Newfoundland and Labrador, St. John's A1B 3X7, Canada*

[7]*Jožef Stefan Institute, Jamova cesta 39, SI-1000 Ljubljana, Slovenia*

[8]*Faculty of Mathematics and Physics, University of Ljubljana, Jadranska ulica 19, SI-1000 Ljubljana, Slovenia*

[9]*RIKEN Center for Emergent Matter Science (CEMS), Wako, Saitama 351-0198, Japan*

[10]*University of Warwick, Department of Physics, Coventry CV4 7AL, United Kingdom*

(Received 3 February 2025; accepted 9 July 2025; published 14 August 2025)

The unabating discovery of nanoskyrmions in centrosymmetric magnets challenges the conventional Dzyaloshinskii-Moriya (DM) skyrmion stabilization mechanism. We investigate Gd_2PdSi_3 using polarized resonant x-ray scattering and find that the low-field incommensurate modulations are elliptical helices, evolving into spin-density waves at higher fields. Quasi-2D magnetism arises via local DM interactions generated by inversion symmetry breaking around Gd-Gd bonds, which we characterize using atomistic simulations. Our findings suggest a prominent "hidden" role of DM interactions even in centrosymmetric skyrmionic hosts.

DOI: 10.1103/td2c-dxgj

The growing interest in topological and emergent phenomena across various areas of condensed matter physics is expanding our understanding of fundamental physical principles while driving innovations in next-generation devices and applications [1,2]. One such phenomenon is the skyrmion, a topologically nontrivial, spatially localized entity emerging in systems with complex competing interactions [3–5]. In magnetic systems, skyrmions manifest as solitonic whirls of magnetization, with a topological vortex-like arrangement of spins conferring protection against their destruction [5–8]. This distinct topology engenders emergent behavior and exceptional dynamical responses, making skyrmions promising candidates for spintronic devices, including neuromorphic, stochastic, and reservoir computing architectures [9–15].

In bulk noncentrosymmetric materials, the competing energies that permit skyrmion formation are the symmetric exchange and antisymmetric Dzyaloshinskii-Moriya (DM) magnetic interactions. This competition results in solitonic solutions for the magnetization, with the relative strength of these interactions determining the length scale of the magnetic textures. The dominating symmetric exchange leads to the formation of long-wavelength (approximately 100 nm) skyrmions, which have been seen in various systems such as B20 helimagnets [16–21], Cu_2OSeO_3 [22–26], and Co-Zn-Mn compounds [27,28]. In these materials, the DM interaction is determined by the symmetry of the crystal, imposing a fixed bulk chirality and configuration to the spin textures [29–31].

Exploring alternative interactions that can stabilize skyrmions is gaining significant momentum. Several theoretical studies predict skyrmion lattices of various morphologies stabilized by the Ruderman-Kittel-Kasuya-Yosida (RKKY) interaction combined with frustration effects on triangular lattices [32–36]. Additionally, skyrmionic solutions have been found by examining the role of biquadratic exchange and four-spin interactions [37–40], which lead to higher-order terms in spatial derivatives reminiscent of the original Skyrme model [3]. These studies are motivating the exploration of $4f$-ion candidate materials, leading to the discovery of nanoscale skyrmions (2–3 nm) in compounds such as Gd_2PdSi_3 [41], $Gd_3Ru_4Al_12$ [42], $GdRu_2Si_2$ [43],

*Contact author: samuel.moody@psi.ch

Published by the American Physical Society under the terms of the Creative Commons Attribution 4.0 International license. Further distribution of this work must maintain attribution to the author(s) and the published article's title, journal citation, and DOI.

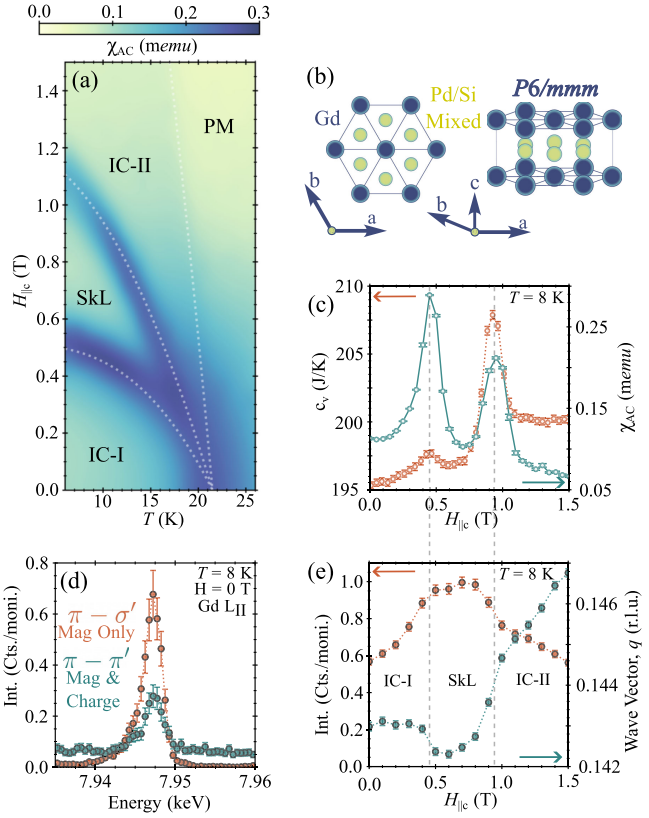

FIG. 1. Characterizing the magnetic textures in Gd_2PdSi_3. (a) Magnetic phase diagram in H-T space, derived from the in-phase component of the ac susceptibility, showing phase regions corresponding to the incommensurate (IC-I/II) magnetic textures, the skyrmion lattice (SkL), and paramagnetic (PM) phase. (b) The reported crystal structure with space group $P6/mmm$ (No. 191). (c) Magnetic field dependence of the magnetic susceptibility (χ_{ac}) and heat capacity (c_V) at 8 K. (d) Polarization-dependent resonant x-ray energy scan of a magnetic satellite reflection, highlighting the presence of a charge-scattering contribution away from resonance. (e) REXS field dependence at 8 K for the integrated intensity and the magnitude of the magnetic wave vector.

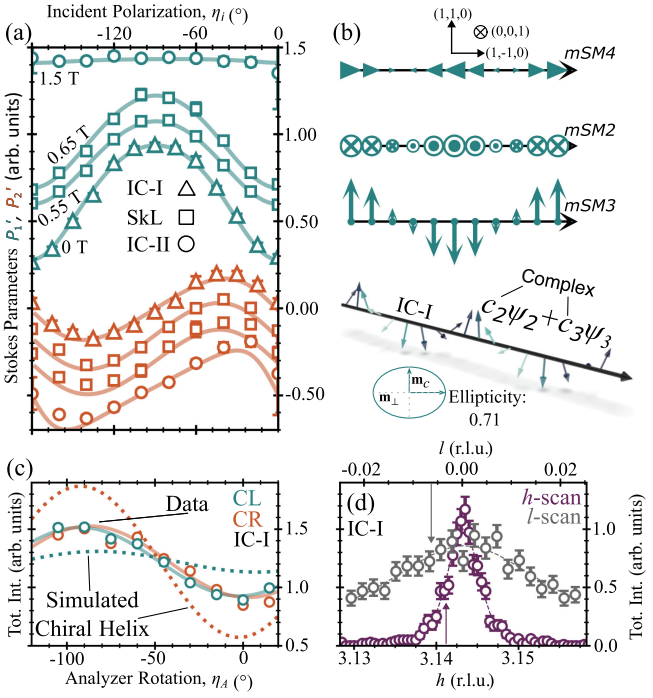

FIG. 2. Determining the magnetic structures in Gd_2PdSi_3. (a) Polarization of the scattered beam, P_1' (teal) and P_2' (orange), for different incoming linear x-ray polarization at 8 K, under applied magnetic fields of 0 T (triangles), 0.55 and 0.65 T (squares), and 1.5 T (circles). Solid lines represent fits with both incoherent charge and magnetic scattering processes. (b) Real-space schematics of the three modes associated to the different irreducible representations, $mSMn$, along with the real-space fitted incommensurate single-q modulation composed of the complex mixing coefficients $c_{2,3}$ at 0 T. (c) Intensity as a function of analyzer rotation, η_A, for circular left (CL) and circular right (CR) incoming x-ray polarization at 0 T. Solid lines show sinusoidal fits to the data. Dotted lines show the simulation of a right-handed helix. (d) Reciprocal space scans of the magnetic satellite along the l (gray) and h (purple) directions.

$Eu(Ga_{1-x}Al_x)_4$ [44–47], and $EuNiGe_3$ [48]. However, the complexity of these crystallographic systems and their subsequent magnetic structures presents challenges in isolating the key interactions responsible for skyrmion stabilization.

In this Letter, we study the paradigmatic centrosymmetric nanoskyrmion-hosting material, Gd_2PdSi_3 [41], exhibiting a complex magnetic phase diagram as seen in Fig. 1(a). At temperatures below 18 K and intermediate magnetic fields, the hexagonal material [Fig. 1(b)] stabilizes a lattice of magnetic skyrmions (SkL) [41]. The SkL is flanked by two other incommensurate (IC) phases: IC-I in lower fields and IC-II at higher applied fields, with clear signatures appearing in susceptibility and heat capacity data at the magnetic transition [Fig. 1(c)]. The nature of these phases remains debated, with the zero-field ground state IC-I being attributed to either spatially separated helical domains [36,41], a lattice of merons and antimerons [41,49,50], or screw-type elliptical helices [51], whereas IC-II is proposed to consist of a magnetic fan, conical, or spin-density-wave (SDW) states [41,50,52]. Resolving the debate on which magnetic interactions are responsible for stabilizing these incommensurate textures first requires a strong understanding of the exact nature of these spin textures. [36,53–57].

To elucidate the relevant physics in Gd_2PdSi_3, we investigate the magnetic structures within a single-crystalline sample (see Ref. [58] for growth information) using resonant elastic x-ray scattering (REXS) at the Gd L_{II} edge at the I16 (Diamond Light Source [59]) and P09 (Deutsches Elektronen-Synchrotron [60]) beamlines, focusing on the magnetic $[3+q,-q,0]$ reflection and magnetic fields along the crystalline c axis. The clear presence of both magnetic and charge-scattering contributions is seen in Fig. 1(d). By performing a full linear x-ray polarization analysis within each phase, we separate these mixed components to

TABLE I. Magnetic structure refinement. Fitted parameters and quality of fit (R_{PS}, more detail in SM [62]) of the single-q components of the magnetic structure model of Gd_2PdSi_3 from the MagStREXS software. The mixing coefficients c_n are associated with basis modes $mSMn$, respectively. The value α accounts for noncoherent charge scattering, and represents the ratio of the charge and magnetic scattering powers, multiplied by their respective scattering populations. Note: these parameters characterize the modulation component at a single wave vector that may be superimposed to form multi-q states, like the SkL.

H (T)	Phase	c_2	c_3	c_4	α	R_{PS}
0	IC-I	$\pm i0.715(10)$	1	0	20.6(11)	5.45
0.55	SkL	$\pm i0.589(7)$	1	0	13.9(13)	4.99
0.65	SkL	$\pm i0.633(14)$	1	0	14.5(16)	7.81
1.50	IC-II	0	1	0	27(9)	5.11

unambiguously determine the magnetic modulations that form the building blocks of the phases. Specifically, the single-q components that may superpose to form the multi-q magnetic structures suggested for this material.

In Fig. 2(a), we present full linear x-ray polarization analysis measurements at 8 K under three different applied fields corresponding to the three magnetic phases [distinguishing features shown in Fig. 1(e)]. Indicative of the compound nature of the scattering processes, the Stokes parameters (P'_1, P'_2) characterizing the outgoing x-ray polarization vary smoothly as a function of the incident x-ray polarization (η_i) in each magnetic phase. Using MagStREXS [61], we separately refine the weights of the charge scattering (α) with the coefficients ($c_{n=2,3,4}$) corresponding to the basis function associated to each magnetic irreducible representation ($mSMn$) obtained from representational analysis. These three modes are SDWs with moments aligned along one single direction [Fig. 2(b)]. See Supplemental Material (SM) [62] for further information and Refs. [63–68].

The optimal parameters for each magnetic phase, summarized in Table I, yield excellent agreement with the data in Fig. 2(a). All observed phases exhibit concomitant charge and magnetic scattering with no $mSM4$ component. In both the IC-I and SkL phases, the single-q magnetic modulations consist of dominant real in-plane $mSM3$ components and weaker imaginary out-of-plane $mSM2$, indicating a distorted elliptical helix with a larger magnetic moment fraction confined to the ab plane. Increasing the magnetic field, we observe a reduction in the overall weight at the IC wave vector, accompanied by the emergence of a ferromagnetic magnetization as more spins align with the external field, as indicated by the increasing net magnetization seen in magnetometry measurements. Concurrently, the ellipticity of the single-q modulation increases, highlighting complex field-induced distortions of nanoskyrmions. A quantitative analysis of these distortions requires a detailed study that accounts for both quadrupolar and interference resonant scattering terms in the REXS cross section, which is beyond

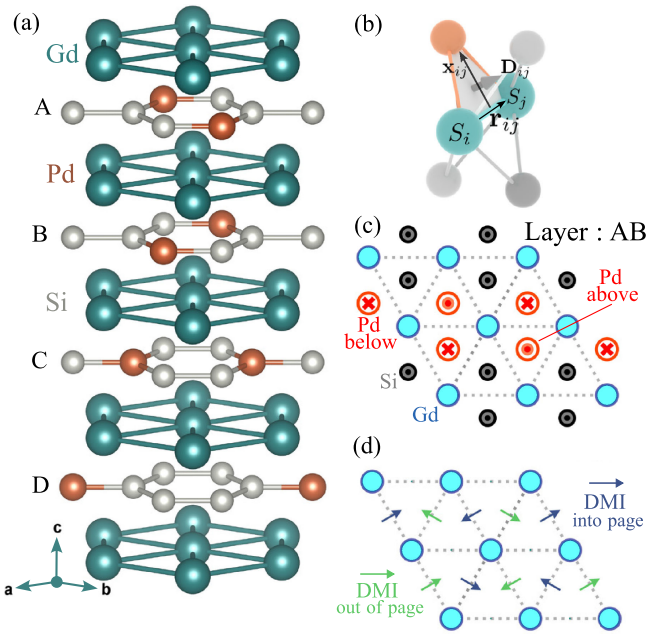

FIG. 3. Crystallographic superstructure and the potential for local Dzyaloshinskii-Moriya (DM) interactions. (a) Crystal structure of Gd_2PdSi_3 showing triangular planes of Gd ions (teal) interleaved with a honeycomb network of Pd (orange) and Si (gray). This forms a crystalline superstructure with eight unit cells stacked along the c axis [69], though only four layers, A-D, are depicted here for clarity. (b) A local DM vector is allowed due to the locally noncentrosymmetric environment surrounding many Gd-Gd bonds. (c) Schematic of a single Gd-Gd layer with an A-type Pd-Si layer above, and a B-type Pd-Si layer below. (d) Resultant symmetry-allowed DM vectors in the Gd-Gd layer. Blue arrows indicate a vector component toward the bottom Pd-Si layer, while green arrows indicate a component toward the top layer.

the scope of this Letter. Comparing across the field-driven magnetic phase transitions, we observe increases in the ellipticity of the single-q modulations, evolving into a SDW-like form in the IC-II phase (in-plane $mSM3$ only). This transformation is driven by the Zeeman interaction, suppressing modulated spin components to stabilize a ferromagnetic component along the applied magnetic field instead.

By analyzing the scattered beam intensity from circularly polarized incident x-rays, we can determine the overall chirality of the magnetism [Fig. 2(c)] in the IC-I phase. Simulating the expected intensities of a right-handed helix (dashed lines) shows a clear difference in the diffracted signal between the circular left (CL) and circular right (CR) polarizations. For a left-handed helix, the behavior of the scattered intensity between the two polarization channels would reverse. Experimentally, negligible dependence is observed upon switching the incident circular polarization, with the intensity lying approximately between the simulated results for CL and CR. This can only be explained by assuming a near equal volume fraction of spatially

separated domains of opposite helix chirality within the sampled volume.

Next we investigate the real-space ordering of the IC-I domains through the reciprocal space scans shown in Fig. 2(d), which display the diffracted intensity as a function of the in-plane (h) and out-of-plane (l) directions. The real-space magnetic correlation lengths, defined as $\xi = [1/\pi](\mathrm{FWHM})^{-1}$, are determined to be $\xi_c = 30(8)$ Å and $\xi_{ab} = 320(30)$ Å for the two directions, respectively. These values align well with a zero-field neutron scattering study [36], where a quadratic-in-l broadening term was required to accurately describe the magnetic Bragg peaks. We see that the correlation length along the crystalline c axis is over an order of magnitude shorter than that in the hexagonal plane, corresponding to roughly the size of a single superstructure cell.

The significance of the anisotropic correlations suggests a quasi-2D nature to the magnetic structures. However, neutron scattering measurements indicate a strong interlayer exchange coupling along the c axis [36], in contrast to the short correlations observed here. Naturally, this raises the question as to the origin of the reduced dimensionality, and suggests a further unexplored mechanism that may provide substantial interlayer frustration.

The role of the ubiquitous crystallographic superstructure in R_2PdSi_3 systems (R is rare earth) has so far been overlooked in most theoretical frameworks. Four layers of distinct Pd-Si ordering are possible, shown in Fig. 3(a). *Ab initio* density functional theory and neutron diffraction studies reveal the optimal stacking sequence comprises alternating layers arranged in a $2 \times 2 \times 8$ superstructure, giving rise to additional crystallographic Bragg reflections [69,70]. Despite the overall centrosymmetric crystal structure, the stacking of different Pd-Si layers results in locally noncentrosymmetric environments surrounding the bond centers between Gd^{3+} ion pairs. This manifests a local DM interaction, characterized by a DM vector, $\mathbf{D}_{ij}$, usually oriented orthogonally to the vector $\mathbf{r}_{ij}$ between the ion pair [71]. An example environment is demonstrated in Fig. 3(b). Various noncentrosymmetric environments exist across a single triangular plane of Gd^{3+} ions between two layers, as shown for one layer (AB) in Fig. 3(c). Depicted in Fig. 3(d), the direction of the DM vectors changes depending on the specific Gd-Gd pair and the stacking configuration, vanishing at bonds surrounded wholly by palladium. See SM [62] for a complete list of all layer combinations and their corresponding DM vectors.

We propose that these local DM interactions drive the observed quasi-2D magnetic ordering, favoring planes of alternating magnetic chirality depending on the specific layer pairing in the superstructure elements, and frustrating the magnetic texture, limiting the out-of-plane magnetic correlation lengths. To test this scenario, we consider a 2D superstructure element with representative AB-layer

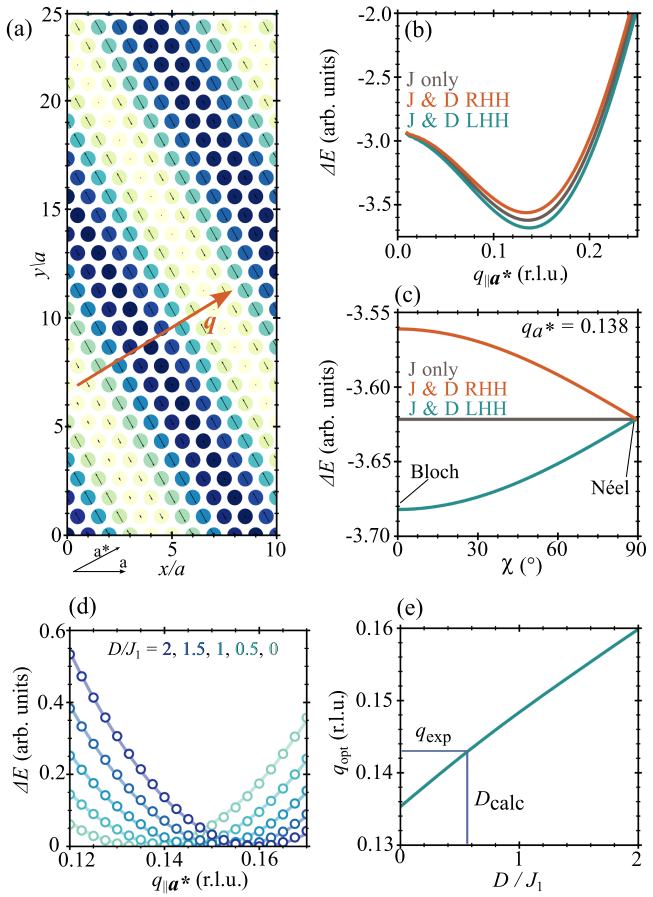

FIG. 4. Two-dimensional atomistic simulations showing the role of the DM interactions. (a) A triangular lattice of Gd^{3+} ions displaying the real-space magnetization texture of the IC-I state. The color represents the out-of-plane component. (b) Magnetic energy of an IC-I spin texture with different handedness as a function of the wave vector along the a^* direction. (c) Magnetic energy of an IC-I spin texture with the $D = 0$ minimum-energy wave vector, plotted as a function of helical helicity, χ. (d) Magnetic energy about the minimum wave vector for different strengths of the DM interaction. (e) Minimum-energy magnetic wave vector as a function of the DM interaction.

stacking (others are shown in SM [62]) using atomistic simulations with an anisotropic spin Hamiltonian,

$$H = -\sum_{\langle i,j \rangle} J_{ij} \mathbf{S}_i \cdot \mathbf{S}_j + \sum_{\langle i,j \rangle} \mathbf{D}_{ij} \cdot (\mathbf{S}_i \times \mathbf{S}_j), \qquad (1)$$

where $\langle i, j \rangle$ denotes pairs of Gd^{3+} ions. We go beyond previous models by including not just experimentally determined nearest-neighbor interactions up to fourth order (J_1, J_2, J_3, and $J_4 = 0.31$, 0.19, 0.27, and -0.21 K [36]), but also bond-dependent DM interactions constrained by local symmetry. The atomistic simulations are performed by simulating a helical texture [Fig. 4(a)] on a 2D 100×100 Gd^{3+} ion lattice, excluding edge sites with incomplete neighbor configurations and demagnetization effects.

The simulations offer invaluable insights into the role of DM interactions within each superstructure element. In Fig. 4(b), we confirm the dominant role of the RKKY interaction in stabilizing the incommensurate magnetism by identifying an energy minimum at $q = 0.138(2)$ r.l.u., comparable to the experimentally observed value [Fig. 1(e)]. Introducing DM interactions lifts the degeneracy between opposite helical chiralities, resulting in a preferred handedness across the entire superstructure layer. Secondly, the DM interactions determine the plane of the spiral winding (Helicity, χ). In an isotropic-exchange-only model, the helical plane remains entirely degenerate, permitting both Bloch-type (moments perpendicular to the wave vector, $\chi = 0$) and Néel-type (moments parallel, $\chi = 90°$) configurations. However, including DM interactions lifts this degeneracy, energetically favoring Bloch-type helices over Néel-type [Fig. 4(c)] in full agreement with our experimental data in Fig. 2(a).

This chiral preference within individual layers underpins the magnetic frustration observed in the system. Namely, certain layers within the superstructure strongly favor a particular chirality. Reversing the local stacking sequence (e.g., from AB to BA), inverts the in-plane orientation of the DM vectors, favoring the opposite chirality for any combination of superstructure layers. However, the global centrosymmetry of the material ensures that both chirality-favoring environments appear in equal proportions throughout the bulk (see SM [62]). As a result, regions of the sample favor opposite-handed configurations, leading to equal chiral-domain volume fractions with the cancellation of any in-plane magnetization summed along the c axis. This cancellation suppresses contrast in Lorentz microscopy, making it ineffective for directly probing the chiral structure. Instead, depth-resolved, surface-sensitive techniques such as resonant elastic x-ray scattering (REXS) at the Eu M_V edge would be particularly valuable for testing this proposal, as they selectively probe only a few atomic layers.

The local DM interactions also affect the periodicity of the magnetic structures, favoring a tighter winding with an increased wave vector. By refining the DM interaction strength, D, such that the simulated wave vector matches the experimental data (i.e., from 0.138 to 0.143 r.l.u.), we constrain the DM interaction to a maximum value of 0.17(1) K within our minimal model, as shown in Figs. 4(d) and 4(e). Although this value is relatively small when compared to the magnetic ordering temperature of 21 K, it significantly influences the magnetism when evaluated relative to J_1. Such a large ratio of $D/J_1 \approx 0.56$ is not unprecedented (for example, in Ni_3TeO_6 [72]). Furthermore, since the strength of J_1 is determined by the RKKY interaction, the lattice spacing could align J_1 near a nodal point of the RKKY interaction, effectively suppressing J_1 and inflating the apparent D/J_1 ratio. Additional experiments, such as inelastic neutron scattering on isotopically enriched single-crystalline samples or electron spin resonance measurements will be essential for confirming this hypothesis quantitatively. Finally, we note that while dipolar interactions are always present, we propose the DM interaction to be the more significant interaction, since the DM scales $DS(S+1) \sim 2.7$ K, compared to the dipolar energy, ~0.5 K, in Gd_2PdSi_3 [73].

Our experimental findings provide new insights into the nature of the magnetic states in centrosymmetric skyrmion hosts. Notably, the ellipticity of the single-q components states implies an inherent real-space variation in the moment, which is unexpected given the localized nature of the Gd^{3+} moment. While itinerant effects or thermal averaging could play a role, the lack of temperature dependence in the ellipticity [51] suggests an alternative explanation: the formation of a triple-q state, where individual single-q components (elliptical helices) superpose to form a 2D lattice [74]. The "missing" x-ray intensity arising from the ellipticity can be accounted for by higher-order diffraction peaks at relevant locations for a 2D magnetic lattice, normalizing the magnitude of the magnetic moment, and consistent with the suggested IC-1 ground state in Gd_2PdSi_3 based on anisotropic spin dynamics [50]. This scenario is further supported by the reduction in hexagonal symmetry due to Pd-Si ordering, which lifts the degeneracy of in-plane wave vectors and provides a potential mechanism for meron-antimeron lattice formation.

In conclusion, using REXS, we have determined that the individual single-q components of the magnetic modulations in the multi-q IC-I and SkL phases of Gd_2PdSi_3 are elliptical Bloch-type helices, while those in the IC-II phase take the form of transverse SDWs. These helical modulations are consistent with separated domains of meron-antimeron and skyrmion lattices. We find that the modulations are chiral, which we attribute to local Dzyaloshinskii-Moriya (DM) interactions induced by the stacking of inequivalent Pd-Si layers in the superlattice structure. Using atomistic simulations, we highlight the role of local atomic environments in stabilizing complex topological spin textures. An intriguing open question is whether similar locally chiral DM interactions play a role in other centrosymmetric nanoskyrmion hosts.

Acknowledgments—We would like to thank J. S. White and other members of the solid state structures group at PSI for helpful discussions. The authors thank DESY (Hamburg, Germany) for beam time on the P09 beamline under Proposal No. I-20191239, and Diamond Light Source (Didcot, UK) for time on beamline I16 under Proposal No. MT20056-1 with the assistance of S. Collins. We thank Raymond Fan and Paul Steadman for the provision of the Quantum Design MPMS3 in the I10 support laboratory, Diamond Light Source. This work was financially supported by the UK Skyrmion Project EPSRC Programme Grant

(No. EP/N032128/1). M. N. W. acknowledges the support of the Natural Sciences and Engineering Research Council of Canada (NSERC). M. G. acknowledges the support of the Slovenian Research and Innovation Agency (ARIS) under Program No. P1-0125, and Projects No. Z1-1852, No. N1-0148, No. J1-2461, No. J1-50008, No. J1-50012, No. N1-0345, No. N1-0356, and No. J2-60034 and EPSRC Grants No. EP/N032128/1 and No. EP/N024028/1.

Data availability—The data that support the findings of this Letter are openly available [75].

[1] M. Z. Hasan and C. L. Kane, Colloquium: Topological insulators, Rev. Mod. Phys. **82**, 3045 (2010).
[2] Xiao Liang Qi and Shou Cheng Zhang, Topological insulators and superconductors, Rev. Mod. Phys. **83**, 1057 (2011).
[3] T. H. R. Skyrme and Basil Ferdinand Jamieson Schonland, A non-linear field theory, Proc. R. Soc. A **260**, 127 (1961).
[4] J. K. Perring and T. H. R. Skyrme, A model unified field equation, Nucl. Phys. **31**, 550 (1962).
[5] Alexei N. Bogdanov and Christos Panagopoulos, Physical foundations and basic properties of magnetic skyrmions, Nat. Rev. Phys. **2**, 492 (2020).
[6] Tom Lancaster, Skyrmions in magnetic materials, Contemp. Phys. **60**, 246 (2019).
[7] Naoto Nagaosa and Yoshinori Tokura, Topological properties and dynamics of magnetic skyrmions, Nat. Nanotechnol. **8**, 899 (2013).
[8] Vivek Lohani, Ciarán Hickey, Jan Masell, and Achim Rosch, Quantum skyrmions in frustrated ferromagnets, Phys. Rev. X **9**, 041063 (2019).
[9] Kyung Mee Song, Jae-Seung Jeong, Biao Pan, Xichao Zhang, Jing Xia, Sunkyung Cha, Tae Eon Park, Kwangsu Kim, Simone Finizio, Jörg Raabe, Joonyeon Chang, Yan Zhou, Weisheng Zhao, Wang Kang, Hyunsu Ju, and Seonghoon Woo, Skyrmion-based artificial synapses for neuromorphic computing, Natl. Electron. Rev. **3**, 148 (2020).
[10] Jakub Zázvorka, Florian Jakobs, Daniel Heinze, Niklas Keil, Sascha Kromin, Samridh Jaiswal, Kai Litzius, Gerhard Jakob, Peter Virnau, Daniele Pinna, Karin Everschor-Sitte, Levente Rózsa, Andreas Donges, Ulrich Nowak, and Mathias Kläui, Thermal skyrmion diffusion used in a reshuffler device, Nat. Nanotechnol. **14**, 658 (2019).
[11] Haoyang Zhang, Daoqian Zhu, Wang Kang, Youguang Zhang, and Weisheng Zhao, Stochastic computing implemented by skyrmionic logic devices, Phys. Rev. Appl. **13**, 054049 (2020).
[12] D. Pinna, G. Bourianoff, and K. Everschor-Sitte, Reservoir computing with random skyrmion textures, Phys. Rev. Appl. **14**, 054020 (2020).
[13] Tomoyuki Yokouchi, Satoshi Sugimoto, Bivas Rana, Shinichiro Seki, Naoki Ogawa, Yuki Shiomi, Shinya Kasai, and Yoshichika Otani, Pattern recognition with neuromorphic computing using magnetic field-induced dynamics of skyrmions, Sci. Adv. **8**, eabq5652 (2022).
[14] Oscar Lee, Tianyi Wei, Kilian D. Stenning, Jack C. Gartside, Dan Prestwood, Shinichiro Seki, Aisha Aqeel, Kosuke Karube, Naoya Kanazawa, Yasujiro Taguchi, Christian Back, Yoshinori Tokura, Will R. Branford, and Hidekazu Kurebayashi, Task-adaptive physical reservoir computing, Nat. Mater. **23**, 79 (2024).
[15] Soju Furuta, Samuel Harrison Moody, Kyohei Kado, Wataru Koshibae, and Fumitaka Kagawa, Energetic perspective on emergent inductance exhibited by magnetic textures in the pinned regime, npj Spintronics **1**, 1 (2023).
[16] S. Mühlbauer, B. Binz, F. Jonietz, C. Pfleiderer, A. Rosch, A. Neubauer, R. Georgii, and P. Böni, Skyrmion lattice in a chiral magnet, Science **323**, 915 (2009).
[17] W. Münzer, A. Neubauer, T. Adams, S. Mühlbauer, C. Franz, F. Jonietz, R. Georgii, P. Böni, B. Pedersen, M. Schmidt, A. Rosch, and C. Pfleiderer, Skyrmion lattice in the doped semiconductor $Fe_{1-x}Co_xSi$, Phys. Rev. B **81**, 041203(R) (2010).
[18] X. Z. Yu, N. Kanazawa, Y. Onose, K. Kimoto, W. Z. Zhang, S. Ishiwata, Y. Matsui, and Y. Tokura, Near room-temperature formation of a skyrmion crystal in thin-films of the helimagnet FeGe, Nat. Mater. **10**, 106 (2011).
[19] Akira Tonomura, Xiuzhen Yu, Keiichi Yanagisawa, Tsuyoshi Matsuda, Yoshinori Onose, Naoya Kanazawa, Hyun Soon Park, and Yoshinori Tokura, Real-space observation of skyrmion lattice in helimagnet MnSi thin samples, Nano Lett. **12**, 1673 (2012).
[20] J. Kindervater, I. Stasinopoulos, A. Bauer, F. X. Haslbeck, F. Rucker, A. Chacon, S. Mühlbauer, C. Franz, M. Garst, D. Grundler, and C. Pfleiderer, Weak crystallization of fluctuating skyrmion textures in MnSi, Phys. Rev. X **9**, 041059 (2019).
[21] L. J. Bannenberg, K. Kakurai, P. Falus, E. Lelièvre-Berna, R. Dalgliesh, C. D. Dewhurst, F. Qian, Y. Onose, Y. Endoh, Y. Tokura, and C. Pappas, Universality of the helimagnetic transition in cubic chiral magnets: Small angle neutron scattering and neutron spin echo spectroscopy studies of FeCoSi, Phys. Rev. B **95**, 144433 (2017).
[22] S. Seki, S. Ishiwata, and Y. Tokura, Magnetoelectric nature of skyrmions in a chiral magnetic insulator Cu_2OSeO_3, Phys. Rev. B **86**, 060403(R) (2012).
[23] M. T. Birch, S. H. Moody, M. N. Wilson, M. Crisanti, O. Bewley, A. Štefančič, G. Balakrishnan, R. Fan, P. Steadman, D. Alba Venero, R. Cubitt, and P. D. Hatton, Anisotropy-induced depinning in the Zn-substituted skyrmion host Cu_2OSeO_3, Phys. Rev. B **102**, 104424 (2020).
[24] M. Crisanti, M. T. Birch, M. N. Wilson, S. H. Moody, A. Štefančič, B. M. Huddart, S. Cabeza, G. Balakrishnan, P. D. Hatton, and R. Cubitt, Position-dependent stability and lifetime of the skyrmion state in nickel-substituted Cu_2OSeO_3, Phys. Rev. B **102**, 224407 (2020).
[25] A. Štefančič, S. H. Moody, T. J. Hicken, M. T. Birch, G. Balakrishnan, S. A. Barnett, M. Crisanti, J. S. O. Evans, S. J. R. Holt, K. J. A. Franke, P. D. Hatton, B. M. Huddart, M. R. Lees, F. L. Pratt, C. C. Tang, M. N. Wilson, F. Xiao, and T. Lancaster, Origin of skyrmion lattice phase splitting in Zn-substituted Cu_2OSeO_3, Phys. Rev. Mater. **2**, 111402(R) (2018).

[26] S. H. Moody, P. Nielsen, M. N. Wilson, D. Alba Venero, A. Štefančič, G. Balakrishnan, and P. D. Hatton, Experimental evidence of a change of exchange anisotropy sign with temperature in Zn-substituted Cu_2OSeO_3, Phys. Rev. Res. **3**, 043149 (2021).

[27] V. Ukleev *et al.*, Frustration-driven magnetic fluctuations as the origin of the low-temperature skyrmion phase in $Co_7Zn_7Mn_6$, npj Quantum Mater. **6**, 40 (2021).

[28] Y. Tokunaga, X. Z. Yu, J. S. White, H. M. Rønnow, D. Morikawa, Y. Taguchi, and Y. Tokura, A new class of chiral materials hosting magnetic skyrmions beyond room temperature, Nat. Commun. **6**, 7638 (2015).

[29] D. Morikawa, K. Shibata, N. Kanazawa, X. Z. Yu, and Y. Tokura, Crystal chirality and skyrmion helicity in MnSi and (Fe, Co)Si as determined by transmission electron microscopy, Phys. Rev. B **88**, 024408 (2013).

[30] David Cortés-Ortuño, Marijan Beg, Vanessa Nehruji, Leoni Breth, Ryan Pepper, Thomas Kluyver, Gary Downing, Thorsten Hesjedal, Peter Hatton, Tom Lancaster, Riccardo Hertel, Ondrej Hovorka, and Hans Fangohr, Proposal for a micromagnetic standard problem for materials with Dzyaloshinskii-Moriya interaction, New J. Phys. **20**, 113015 (2018).

[31] A. N. Bogdanov, U. K. Rößler, M. Wolf, and K.-H. Müller, Magnetic structures and reorientation transitions in noncentrosymmetric uniaxial antiferromagnets, Phys. Rev. B **66**, 214410 (2002).

[32] Kota Mitsumoto and Hikaru Kawamura, Skyrmion crystal in the RKKY system on the two-dimensional triangular lattice, Phys. Rev. B **105**, 094427 (2022).

[33] Zhentao Wang, Ying Su, Shi-Zeng Lin, and Cristian D. Batista, Skyrmion crystal from RKKY interaction mediated by 2D electron gas, Phys. Rev. Lett. **124**, 207201 (2020).

[34] Ryota Yambe and Satoru Hayami, Skyrmion crystals in centrosymmetric itinerant magnets without horizontal mirror plane, Sci. Rep. **11**, 11184 (2021).

[35] Tsuyoshi Okubo, Sungki Chung, and Hikaru Kawamura, Multiple-q states and the skyrmion lattice of the triangular-lattice Heisenberg antiferromagnet under magnetic fields, Phys. Rev. Lett. **108**, 017206 (2012).

[36] Joseph A. M. Paddison, Binod K. Rai, Andrew F. May, Stuart Calder, Matthew B. Stone, Matthias D. Frontzek, and Andrew D. Christianson, Magnetic interactions of the centrosymmetric skyrmion material Gd_2PdSi_3, Phys. Rev. Lett. **129**, 137202 (2022).

[37] Alexey Kartsev, Mathias Augustin, Richard F. L. Evans, Kostya S. Novoselov, and Elton J. G. Santos, Biquadratic exchange interactions in two-dimensional magnets, npj Comput. Mater. **6**, 150 (2020).

[38] Souvik Paul, Soumyajyoti Haldar, Stephan von Malottki, and Stefan Heinze, Role of higher-order exchange interactions for skyrmion stability, Nat. Commun. **11**, 4756 (2020).

[39] Stefan Heinze, Kirsten von Bergmann, Matthias Menzel, Jens Brede, André Kubetzka, Roland Wiesendanger, Gustav Bihlmayer, and Stefan Blügel, Spontaneous atomic-scale magnetic skyrmion lattice in two dimensions, Nat. Phys. **7**, 713 (2011).

[40] A. Lászlóffy, L. Rózsa, K. Palotás, L. Udvardi, and L. Szunyogh, Magnetic structure of monatomic Fe chains on Re(0001): Emergence of chiral multispin interactions, Phys. Rev. B **99**, 184430 (2019).

[41] Takashi Kurumaji, Taro Nakajima, Max Hirschberger, Akiko Kikkawa, Yuichi Yamasaki, Hajime Sagayama, Hironori Nakao, Yasujiro Taguchi, Takahisa Arima, and Yoshinori Tokura, Skyrmion lattice with a giant topological Hall effect in a frustrated triangular-lattice magnet, Science **365**, 914 (2019).

[42] Max Hirschberger, Taro Nakajima, Shang Gao, Licong Peng, Akiko Kikkawa, Takashi Kurumaji, Markus Kriener, Yuichi Yamasaki, Hajime Sagayama, Hironori Nakao, Kazuki Ohishi, Kazuhisa Kakurai, Yasujiro Taguchi, Xiuzhen Yu, Takahisa Arima, and Yoshinori Tokura, Skyrmion phase and competing magnetic orders on a breathing kagomé lattice, Nat. Commun. **10**, 5831 (2019).

[43] Nguyen Duy Khanh, Taro Nakajima, Xiuzhen Yu, Shang Gao, Kiyou Shibata, Max Hirschberger, Yuichi Yamasaki, Hajime Sagayama, Hironori Nakao, Licong Peng, Kiyomi Nakajima, Rina Takagi, Takahisa Arima, Yoshinori Tokura, and Shinichiro Seki, Nanometric square skyrmion lattice in a centrosymmetric tetragonal magnet, Nat. Nanotechnol. **15**, 444 (2020).

[44] Rina Takagi, Naofumi Matsuyama, Victor Ukleev, Le Yu, Jonathan S. White, Sonia Francoual, José R. L. Mardegan, Satoru Hayami, Hiraku Saito, Koji Kaneko, Kazuki Ohishi, Yoshichika Ōnuki, Takahisa Arima, Yoshinori Tokura, Taro Nakajima, and Shinichiro Seki, Square and rhombic lattices of magnetic skyrmions in a centrosymmetric binary compound, Nat. Commun. **13**, 1472 (2022).

[45] Jaime M. Moya, Shiming Lei, Eleanor M. Clements, Caitlin S. Kengle, Stella Sun, Kevin Allen, Qizhi Li, Y. Y. Peng, Ali A. Husain, Matteo Mitrano, Matthew J. Krogstad, Raymond Osborn, Anand B. Puthirath, Songxue Chi, L. Debeer-Schmitt, J. Gaudet, P. Abbamonte, Jeffrey W. Lynn, and E. Morosan, Incommensurate magnetic orders and topological Hall effect in the square-net centrosymmetric $EuGa_2Al_2$ system, Phys. Rev. Mater. **6**, 074201 (2022).

[46] M. T. Littlehales, S. H. Moody, P. J. Bereciartua, D. A. Mayoh, Z. B. Parkin, T. J. Blundell, E. Unsworth, S. Francoual, G. Balakrishnan, D. A. Venero, and P. D. Hatton, Spin density waves and ground state helices in $EuGA_{2.4}Al_{1.6}$, Phys. Rev. Res. **6**, L032015 (2024).

[47] Kelly J. Neubauer, Kevin Allen, Jaime M. Moya, Mason L. Klemm, Feng Ye, Zachary Morgan, Lisa DeBeer-Schmitt, Wei Tian, Emilia Morosan, and Pengcheng Dai, Correlation between complex spin textures and the magnetocaloric and Hall effects in $Eu(Ga_{1-x}Al_x)_4$ $(x = 0.9, 1)$. Phys. Rev. B **111**, 165136 (2025).

[48] Deepak Singh, Yukako Fujishiro, Satoru Hayami, Samuel H. Moody, Takuya Nomoto, Priya R. Baral, Victor Ukleev, Robert Cubitt, Nina-Juliane Steinke, Dariusz J. Gawryluk, Ekaterina Pomjakushina, Yoshichika Ōnuki, Ryotaro Arita, Yoshinori Tokura, Naoya Kanazawa, and Jonathan S. White, Transition between distinct hybrid skyrmion textures through their hexagonal-to-square crystal transformation in a polar magnet, Nat. Commun. **14**, 8050 (2023).

[49] M. Hirschberger, L. Spitz, T. Nomoto, T. Kurumaji, S. Gao, J. Masell, T. Nakajima, A. Kikkawa, Y. Yamasaki, H. Sagayama, H. Nakao, Y. Taguchi, R. Arita, T. H. Arima,

and Y. Tokura, Topological Nernst effect of the two-dimensional skyrmion lattice, Phys. Rev. Lett. **125**, 076602 (2020).

[50] M. Gomilšek, T. J. Hicken, M. N. Wilson, K. J. A. Franke, B. M. Huddart, A. Štefančič, S. J. R. Holt, G. Balakrishnan, D. A. Mayoh, M. T. Birch, S. H. Moody, H. Luetkens, Z. Guguchia, M. T. F. Telling, P. J. Baker, S. J. Clark, and T. Lancaster, Anisotropic skyrmion and multi-q spin dynamics in centrosymmetric Gd_2PdSi_3, Phys. Rev. Lett. **134**, 046702 (2025).

[51] J. Ju, H. Saito, T. Kurumaji, M. Hirschberger, A. Kikkawa, Y. Taguchi, T. Arima, Y. Tokura, and T. Nakajima, Polarized neutron scattering study of the centrosymmetric skyrmion host material Gd_2PdSi_3, Phys. Rev. B **107**, 024405 (2022).

[52] S. H. Moody, M. N. Wilson, M. T. Birch, M. Gomilšek, S. P. Collins, A. Štefančič, G. Balakrishnan, and P. D. Hatton, Charge Density Waves and Coplanar Magnetism in Gd_2PdSi_3, arXiv:2010.14326.

[53] Takuya Nomoto, Takashi Koretsune, and Ryotaro Arita, Formation mechanism of the helical q structure in Gd-based skyrmion materials, Phys. Rev. Lett. **125**, 117204 (2020).

[54] J. Bouaziz, E. Mendive-Tapia, S. Blügel, and J. B. Staunton, Fermi-surface origin of skyrmion lattices in centrosymmetric rare-earth intermetallics, Phys. Rev. Lett. **128**, 157206 (2022).

[55] Satoru Hayami, Ryo Ozawa, and Yukitoshi Motome, Effective bilinear-biquadratic model for noncoplanar ordering in itinerant magnets, Phys. Rev. B **95**, 224424 (2017).

[56] A. O. Leonov and M. Mostovoy, Multiply periodic states and isolated skyrmions in an anisotropic frustrated magnet, Nat. Commun. **6**, 8275 (2015).

[57] Shi-Zeng Lin and Satoru Hayami, Ginzburg-landau theory for skyrmions in inversion-symmetric magnets with competing interactions, Phys. Rev. B **93**, 064430 (2016).

[58] D. A. Mayoh, A. Štefančič, M. R. Lees, and G. Balakrishnan, Crystal growth of the R_2PdSi_3 (R = rare earth) materials using the optical floating zone technique, J. Cryst. Growth **642**, 127774 (2024).

[59] S. P. Collins, A. Bombardi, A. R. Marshall, J. H. Williams, G. Barlow, A. G. Day, M. R. Pearson, R. J. Woolliscroft, R. D. Walton, G. Beutier, and G. Nisbet, Diamond beamline I16 (materials and magnetism), AIP Conf. Proc. **1234**, 303 (2010).

[60] J. Strempfer, S. Francoual, D. Reuther, D. K. Shukla, A. Skaugen, H. Schulte-Schrepping, T. Kracht, and H. Franz, Resonant scattering and diffraction beamline P09 at PETRA III, J. Synchrotron Radiat. **20**, 541 (2013).

[61] Pablo J. Bereciartua, Juan Rodríguez-Carvajal, and Sonia Francoual, MagStREXS: Crystallographic software for magnetic structure determination through resonant x-ray magnetic diffraction data, Acta Crystallogr. Sect. A **77**, C177 (2021).

[62] See Supplemental Material at http://link.aps.org/supplemental/10.1103/td2c-dxgj for additional details on polarization analysis and beam polarization characteristics, experimental methods, and atomistic simulation procedures.

[63] S. R. Saha, H. Sugawara, T. D. Matsuda, Y. Aoki, H. Sato, and E. V. Sampathkumaran, Resistivity minimum and anisotropy in R_2PdSi_3 (R = Ce, Gd). Physica B (Amsterdam) **281-282**, 116 (2000).

[64] G. D. A. Wood, D. D. Khalyavin, D. A. Mayoh, J. Bouaziz, A. E. Hall, S. J. R. Holt, F. Orlandi, P. Manuel, S. Blügel, J. B. Staunton, O. A. Petrenko, M. R. Lees, and G. Balakrishnan, Double-q ground state with topological charge stripes in the centrosymmetric skyrmion candidate $GdRu_2Si_2$, Phys. Rev. B **107**, L180402 (2023).

[65] Yuuki Yasui, Christopher J. Butler, Nguyen Duy Khanh, Satoru Hayami, Takuya Nomoto, Tetsuo Hanaguri, Yukitoshi Motome, Ryotaro Arita, Takahisa Arima, Yoshinori Tokura, and Shinichiro Seki, Imaging the coupling between itinerant electrons and localised moments in the centrosymmetric skyrmion magnet $GdRu_2Si_2$, Nat. Commun. **11**, 5925 (2020).

[66] A. Gerrard and J. M. Burch, *Introduction to Matrix Methods in Optics*, Dover Books on Physics (Dover, New York, 1994).

[67] C. Detlefs, M. Sanchez del Rio, and C. Mazzoli, X-ray polarization: General formalism and polarization analysis, Eur. Phys. J. Special Topics **208**, 359 (2012).

[68] Wolfgang Simeth, Andreas Bauer, Christian Franz, Aisha Aqeel, Pablo J. Bereciartua, Jennifer A. Sears, Sonia Francoual, Christian H. Back, and Christian Pfleiderer, Resonant elastic x-ray scattering of antiferromagnetic superstructures in $EuPtSi_3$, Phys. Rev. Lett. **130**, 266701 (2023).

[69] Fei Tang, Matthias Frontzek, Julia Dshemuchadse, Tilmann Leisegang, Matthias Zschornak, Robert Mietrach, Jens-Uwe Hoffmann, Wolfgang Löser, Sibylle Gemming, Dirk C. Meyer, and Michael Loewenhaupt, Crystallographic superstructure in R_2PdSi_3 compounds (R = heavy rare earth), Phys. Rev. B **84**, 104105 (2011).

[70] Leonie Spitz, Takuya Nomoto, Shunsuke Kitou, Hironori Nakao, Akiko Kikkawa, Sonia Francoual, Yasujiro Taguchi, Ryotaro Arita, Yoshinori Tokura, Takahisa Arima, and Max Hirschberger, Entropy-assisted, long-period stacking of honeycomb layers in an AlB2-type silicide, J. Am. Chem. Soc. **144**, 16866 (2022).

[71] I. Dzyaloshinsky, A thermodynamic theory of "weak" ferromagnetism of antiferromagnetics, J. Phys. Chem. Solids **4**, 241 (1958).

[72] Jakob Lass, Chiral magnons in multiferroic Ni_3TeO6, *European Conference on Neutron Scattering* (Technical University of Munich, Garching, 2023).

[73] S. Blundell, *Magnetism in Condensed Matter*, Oxford Master Series in Condensed Matter Physics (OUP, Oxford, 2001).

[74] Satoru Hayami, Tsuyoshi Okubo, and Yukitoshi Motome, Phase shift in skyrmion crystals, Nat. Commun. **12**, 6927 (2021).

[75] S. H. Moody, P. J. Bereciartua, S. Francoual, M. T. Littlehales, M. N. Wilson, M. Gomilšek, M. T. Birch, D. A. Mayoh, G. Balakrishnan, and P. D. Hatton, Zenodo (2025), https://zenodo.org/records/16738732.